On the nucleation of amyloid β-protein monomer folding

NOEL D. LAZO,[1] MARIANNE A. GRANT,[2] MARGARET C. CONDRON,[1] ALAN C. RIGBY,[2] AND DAVID B. TEPLOW[1]

[1]Department of Neurology, David Geffen School of Medicine at UCLA, Los Angeles, California 90095, USA
[2]Division of Hemostasis and Thrombosis, Beth Israel Deaconess Medical Center, and Department of Medicine, Harvard Medical School, Boston, Massachusetts 02215, USA

(RECEIVED December 16, 2004; FINAL REVISION February 18, 2005; ACCEPTED February 18, 2005)

Abstract

Neurotoxic assemblies of the amyloid β-protein (Aβ) have been linked strongly to the pathogenesis of Alzheimer's disease (AD). Here, we sought to monitor the earliest step in Aβ assembly, the creation of a folding nucleus, from which oligomeric and fibrillar assemblies emanate. To do so, limited proteolysis/mass spectrometry was used to identify protease-resistant segments within monomeric Aβ(1–40) and Aβ(1–42). The results revealed a 10-residue, protease-resistant segment, Ala21–Ala30, in both peptides. Remarkably, the homologous decapeptide, Aβ(21–30), displayed identical protease resistance, making it amenable to detailed structural study using solution-state NMR. Structure calculations revealed a turn formed by residues Val24–Lys28. Three factors contribute to the stability of the turn, the intrinsic propensities of the Val-Gly-Ser-Asn and Gly-Ser-Asn-Lys sequences to form a β-turn, long-range Coulombic interactions between Lys28 and either Glu22 or Asp23, and hydrophobic interaction between the isopropyl and butyl side chains of Val24 and Lys28, respectively. We postulate that turn formation within the Val24–Lys28 region of Aβ nucleates the intramolecular folding of Aβ monomer, and from this step, subsequent assembly proceeds. This model provides a mechanistic basis for the pathologic effects of amino acid substitutions at Glu22 and Asp23 that are linked to familial forms of AD or cerebral amyloid angiopathy. Our studies also revealed that common C-terminal peptide segments within Aβ(1–40) and Aβ(1–42) have distinct structures, an observation of relevance for understanding the strong disease association of increased Aβ(1–42) production. Our results suggest that therapeutic approaches targeting the Val24–Lys28 turn or the Aβ(1–42)-specific C-terminal fold may hold promise.

Keywords: Alzheimer's disease; amyloid; amyloid β-protein; folding nucleus; protein folding

Supplemental material: see www.proteinscience.org

Reprint requests to: David B. Teplow, Department of Neurology, David Geffen School of Medicine at UCLA, 710 Westwood Plaza (Reed C119A), Los Angeles, CA 90095, USA; e-mail: dteplow@mednet.ucla.edu; fax: (310) 206-1700.

Abbreviations: Aβ, amyloid β-protein; CT, chymotrypsin; DQF-COSY, double-quantum filtered correlation spectroscopy; Asp-N, endoproteinase AspN; GluC, endoproteinase Glu-C; HNE, human neutrophil elastase; NOESY, nuclear Overhauser enhancement spectroscopy; PPE, porcine pancreatic elastase; RP-HPLC, reverse-phase high-performance liquid chromatography; ROESY, rotating-frame Overhauser enhancement spectroscopy; TH, thermolysin; TOCSY, total correlation spectroscopy; TR, trypsin.

Article and publication are at http://www.proteinscience.org/cgi/doi/10.1110/ps.041292205.

The amyloid β-protein (Aβ) is a normal, soluble component of human plasma and cerebrospinal fluid (Haass et al. 1992; Seubert et al. 1992; Shoji et al. 1992). Aβ exists predominantly as a 40- or 42-residue peptide (for review, see Teplow 1998). Historically, the assembly of Aβ into amyloid fibrils was thought to initiate a pathogenic cascade resulting in AD (the amyloid cascade hypothesis) (Hardy and Allsop 1991). However, progressively smaller assemblies have been discovered (Oda et al. 1995; Harper et al. 1997; Walsh et al. 1997; Lambert et al. 1998; Bitan et al. 2003a), and each has been found to be neurotoxic (Lambert et al. 1998; Hartley et al. 1999; Walsh et al. 1999;

Sun et al. 2003; Taylor et al. 2003). This accumulating evidence supports a revision of the amyloid cascade hypothesis such that Aβ assembly into neurotoxic oligomers, and not into fibrils, is the seminal event in AD pathogenesis (Haass and Steiner 2001; Klein et al. 2001, 2004; Kirkitadze et al. 2002; Walsh et al. 2002). If the hypothesis is true, then preventing the folding of nascent Aβ monomer into toxic conformers or oligomers would have therapeutic benefit.

Certain regions of Aβ exert strong control over assembly kinetics and biological activity. The dipeptide Ile41–Ala42 at the C terminus of Aβ, which distinguishes Aβ(1–42) from Aβ(1–40), is responsible for distinct biophysical (Jarrett et al. 1993; Bitan et al. 2003a), physiologic (Klein et al. 2004), and clinical (Iwatsubo et al. 1995) behaviors of the longer peptide. These behaviors include oligomerization into pentamer/hexamer units (paranuclei) (Bitan et al. 2003a), nucleation of amyloid formation from shorter variants such as Aβ(1–39) and Aβ(1–40) (Jarrett et al. 1993), formation of Aβ-derived diffusible ligands (ADDLs) (Oda et al. 1995; Lambert et al. 1998), early deposition in senile plaques in Down's syndrome patients (Iwatsubo et al. 1995), and strong linkage to AD (Younkin 1995). Amino acid substitutions within and adjacent to the central hydrophobic cluster (CHC) of Aβ, Leu17–Ala21, cause cerebral amyloid angiopathy and AD-like diseases (Levy et al. 1990; Kamino et al. 1992; Hendriks and Vanbroeckhoven 1996; Tagliavini et al. 1999; Grabowski et al. 2001; Nilsberth et al. 2001). In vitro studies have probed the biophysical consequences of these mutations. For example, the Glu22→Gln substitution increases both the rates of nucleation and elongation of Aβ fibrils (Wisniewski et al. 1991; Teplow et al. 1997) and the Glu22→Gly substitution facilitates protofibril formation (Nilsberth et al. 2001; Päiviö et al. 2004). Met35 may be important both in Aβ-associated redox chemistry (Butterfield 2002) and in the peptide assembly (Snyder et al. 1994; Seilheimer et al. 1997; Watson et al. 1998; Butterfield 2002; Hou et al. 2002a; Palmblad et al. 2002). Recent studies suggest that formation of methionine sulfoxide (Met[O]) or methionine sulfone (Met[O_2]) block oligomerization of Aβ(1–42), preventing fibril assembly (Hou et al. 2002b; Palmblad et al. 2002; Bitan et al. 2003b). Taken together, these data have revealed how small changes in Aβ primary structure can alter intermolecular interactions among Aβ monomers.

To examine assembly-dependent features of intramolecular peptide organization, Aβ secondary structure characteristics have been determined spectroscopically. The conformational changes occurring during fibril assembly involve random coil (RC)→α-helix, RC→β-strand, and α-helix→β-strand transitions (Barrow et al. 1992; Soto et al. 1995; Sticht et al. 1995; Coles et al. 1998; Shao et al. 1999; Walsh et al. 1999; Zagorski et al. 2000; Zhang et al. 2000; Kirkitadze et al. 2001). The involvement of turn elements early in fibril formation is less clear. Studies of Aβ fragments, including Aβ(19–28) (Gorevic et al. 1987; Sorimachi et al. 1990), Aβ(15–28) (Gorevic et al. 1987), and Aβ(25–35) (Laczko et al. 1994), suggest turns are present. However, no turns were found in studies of Aβ(10–35) fibrils (Benzinger et al. 2000). In contrast, modeling based on established examples of β-helical conformation, and on hydrophobic and hydrogen bonding effects on protein folding, suggests a β-turn at Val24–Asn27 (Lazo and Downing 1998). In silico modeling of fibrils from Aβ(1–43) reveals a β-turn at Gly25–Lys28 (George and Howlett 1999). Solid-state NMR studies of Aβ(1–40) fibrils suggest a bend at Gly25–Gly29 (Petkova et al. 2002).

As illustrated above, a deepening understanding of Aβ peptide oligomerization and fibril formation is being obtained. The aim of the work reported here was to establish how these important assembly processes are initiated at the monomer level. To do so, we probed the conformation of Aβ monomer using limited proteolysis (Fontana et al. 1997; Hubbard 1998) in combination with mass spectrometry. This approach is useful in the study of conformational changes in proteins that have a strong propensity to aggregate (Kheterpal et al. 2001; Polverino de Laureto et al. 2003; Monti et al. 2004). Results suggest, in both Aβ(1–40) and Aβ(1–42), that a nucleus for intramolecular folding exists within the decapeptide region Ala21–Ala30. Solution-state NMR studies of the corresponding Aβ(21–30) decapeptide revealed a turn element formed by residues Val24–Lys28 and provided a resolved structure of the nucleus.

Results

Limited proteolysis of Aβ(1–40) and Aβ(1–42)

Limited proteolysis under nondenaturing conditions was used (Fontana et al. 1997; Hubbard 1998) in combination with liquid chromatography/mass spectrometry (LC/MS) to determine protease-accessible sites in Aβ(1–40) and Aβ(1–42). Endoproteinases were selected (Table 1) that were capable, theoretically, of cleaving 38/39 and 40/41 peptide bonds within Aβ(1–40) and Aβ(1–42), respectively (Fig. 1). Most peptide bonds were substrates for two or more proteases. To specifically identify unstructured regions of Aβ prior to self-assembly, low enzyme: substrate (E:S) ratios (1:1000 to 1:100) and short digestion times (1–5 min) were used to digest low molecular weight (LMW) Aβ (Walsh et al. 1999; Bitan et al. 2001) and the digestions were performed at 25°C (to inhibit peptide assembly) (Gursky and Aleshkov 2000). We have shown previously that LMW Aβ comprises monomers in equilibrium with metastable, low-order oligomers (Bitan et al.

Table 1. *Endoproteinase substrate specificity*

Proteinase	EC Number	Specificity (P_1-P_1')[a]
Chymotrypsin (CT)	3.4.21.1	P_1 = Tyr, Phe, Leu, Met, Trp
Endoproteinase Asp-N (AspN)	3.4.24.33	P_1' = Asp
Endoproteinase Glu-C (GluC)	3.4.21.19	P_1 = Glu, Asp (minor)
Human neutrophil elastase (HNE)	3.4.21.37	P_1 = Ala, Val (major), Leu, Ile, Ser, Gly
Porcine pancreatic elastase (PPE)	3.4.21.36	P_1 = Ala, Val, Leu, Ile, Ser, Gly
Thermolysin (TH)	3.4.24.27	$P_1' \neq$ Asp, Cys, Gln, Pro, Trp
Trypsin (TR)	3.4.21.4	P_1 = Arg, Lys

[a] Nomenclature for amino acids neighboring the scissile peptide bond is that of Schechter and Berger (1967).

2003a). In the experiments reported here, the protease substrate was predominantly the peptide monomer (see Discussion). Data interpretation was straightforward and produced quite large data sets. A representative experiment and a summary of results from all experiments are presented below. All other experimental data are provided in the Supplemental Material.

Thermolysin (TH)

Results from treatment of Aβ(1–40) with thermolysin (TH), a nonspecific protease, are illustrated in Figure 2. After 1 min, fragments 1–16, 1–17, 1–18, 1–19, 1–30, and 1–33 were detected, along with small amounts of 17–40, 18–40, 19–40, 20–40, 31–40, and 34–40. These data indicated initial cleavages at the peptide bonds between Lys16 and Leu17, Leu17 and Val18, Val18 and Phe19, Phe19 and Phe20, Ala30 and Ile31, and Gly33 and Leu34, respectively (Fig. 2; Table 2). Almost all of Aβ(1–40) was digested by 30 min and its digestion was complete by 60 min. At 60 min, the most abundant fragments were 4–11, 12–17, 20–33, and 34–40. Significant amounts of fragments 20–29 and 20–30 now were observed. The amounts of the 20–29 and 20–30 fragments continued increasing during 24 h of incubation so that at the end of this period these fragments, along with 4–11, 12–17, 20–33, and 34–40, were most abundant. The continued observation of these fragments after prolonged incubation using an E:S ratio of 1:1000 suggests that they are relatively resistant to proteolytic digestion. However, these fragments can be digested. After 4 d of incubation at an E:S ratio of 1:10, fragments 20–33 and 34–40 were no longer detectable by LC/MS (data not shown). The amount of fragment 4–11, as indicated by peak area, also decreased. The 12–17 fragment eluted very close to the injection peak; therefore, it was not possible to determine if the absorbance of the fragment also decreased. However, the width of the injection peak increased during the incubation, suggesting short peptide fragments were produced. Increased production of the 20–29 and 20–28 fragments, and the observation of the 20–24 fragment near the injection peak, demonstrated that digestion of the 20–30 fragment occurred. In these latter experiments, the rank order of peptide bond lability was identical to that observed using lower E:S ratios. Thus, fragments 20–29 and 20–30 were produced only after almost all of the large fragments had been digested. Fragment 20–30 eluted aberrantly from the C18 column used in the chromatography (Fig. 2, 24-h sample). Compared to the elution peaks of the other fragments, the peak shape of fragment 20–30 was not sharp. Maximum amounts of the fragment 20–30 peak were observed spectrophotometrically at a retention time of 6.5 min, but ions ($(M + 2H)^{2+}$ = 547.9 and $(M + H)^{+}$ = 1094.9) of the fragment were observed in the total ion chromatogram until 18 min. Study of Aβ(1–42) revealed the same six initial sites of endoproteolysis as observed in Aβ(1–40) (see Supplemental Material, Fig. S1).

Proteolysis by other proteases

Digestions of Aβ(1–40) and Aβ(1–42) also were carried out using chymotrypsin (CT, Supplemental Fig. S2), endoproteinase Asp-N (AspN, Supplemental Fig. S3), endo-

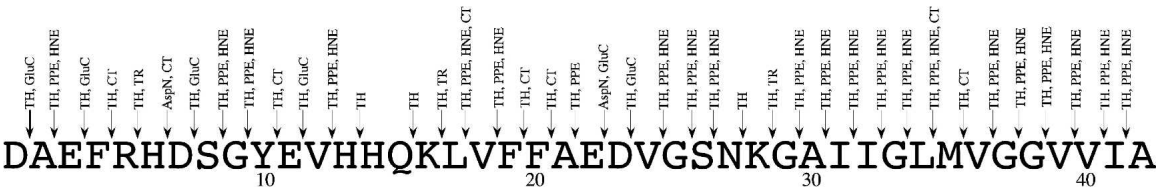

Figure 1. Potential endoproteinase cleavage sites. Arrows indicate potential sites of peptide bond cleavage by the indicated endoproteinases. Abbreviations: chymotrypsin, CT; endoproteinase Asp-N, AspN; endoproteinase Glu-C, GluC; human neutrophil elastase, HNE; porcine pancreatic elastase, PPE; thermolysin, TH; trypsin, TR.

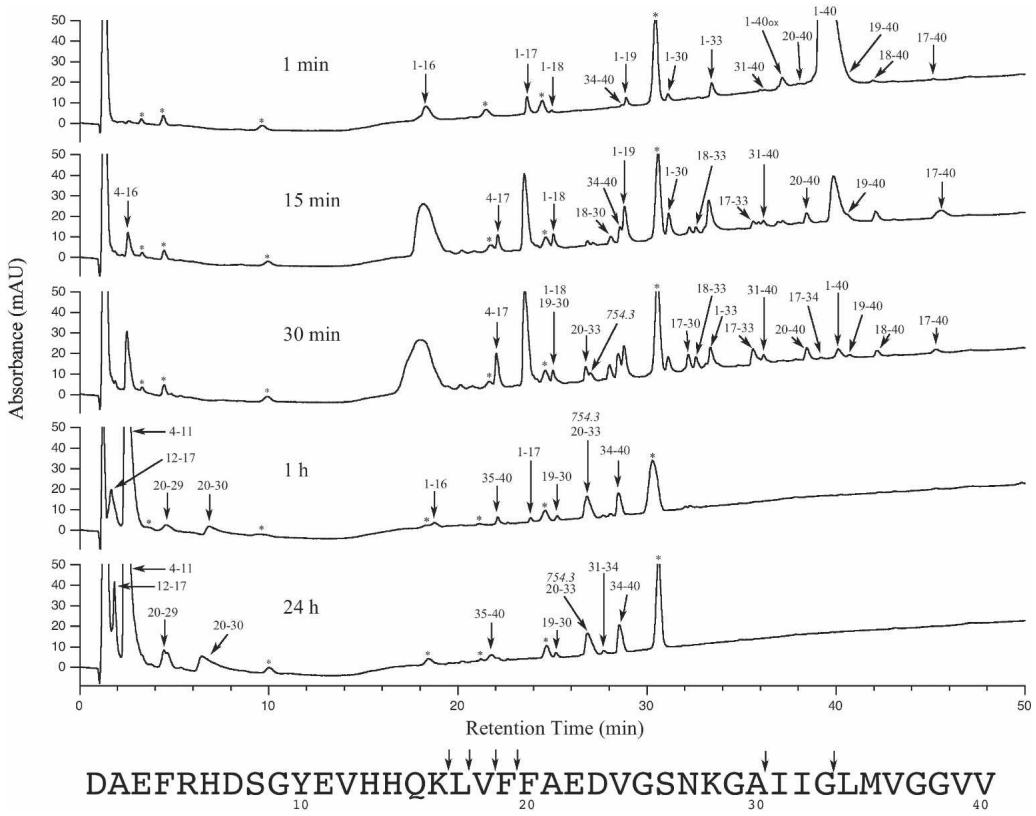

Figure 2. Limited proteolysis of Aβ by thermolysin (TH). LMW Aβ(1–40) at a concentration of 92 μM was digested by TH using an E:S ratio of 1:1000. Chromatograms are shown of samples removed at the indicated times and subjected to LC/MS analysis. The peptides comprising each peak are noted above arrows designating the corresponding peaks. In cases in which observed masses could not be assigned to specific peptides, the actual mass is noted in italics. In this and all other chromatograms, the suffix "ox," as in "1–40ox," signifies an oxidized form of Aβ which produces ions 16 Da larger than predicted. During peptide synthesis and experimental study, oxidation of Aβ occurs commonly at Met35 in a low percentage of molecules, producing Met35(O) (unpublished). This phenomenon explains why full-length Aβ and Aβ fragments containing Met35 are observed at higher mass than expected. Asterisks denote peaks present in undigested peptide samples. Chromatograms were obtained using a C18 column. Below the chromatograms, sites of initial peptide bond cleavage are indicated by arrows above the amino acid sequence.

proteinase Glu-C (GluC, Supplemental Fig. S4), human neutrophil elastase (HNE, Supplemental Fig. S5), porcine pancreatic elastase (PPE, Supplemental Fig. S6), and trypsin (TR, Supplemental Fig. S7). In each case, temporal changes in peptide maps were observed and mass spectrometric analysis of digests revealed the positions of susceptible peptide bonds (Tables 2, 3). A summary of the data from all proteolysis experiments is presented in Figure 3. The data show that both Aβ(1–40) and Aβ(1–42) have protease-sensitive peptide bonds in their N termini, central hydrophobic clusters (CHC; Leu17–Ala21), and C termini. Fifteen of 16 sites were identical. The Val39–Val40 peptide bond is cleaved by PPE in Aβ(1–40) but not in Aβ(1–42). If each peptide is digested with HNE in the presence of 5 M Gu•HCl, the Leu34–Met35 bond is cleaved in both peptides and the Val40–Ile41 bond is cleaved in Aβ(1–42) (Supplemental Fig. S5). These data suggest that the C terminus of Aβ(1–42), in the absence of denaturant, may exist in a structured state (e.g., involving a Gly37–Gly38 turn) (Lazo and Downing 1998, 1999; Grant et al. 2000; Gibbs et al. 2002). Protease-mediated peptide bond cleavage requires structural flexibility at least among residues P2–P1–P1′–P2′ (Schechter and Berger 1967; Hubbard 1998). The most prominent feature of the map of protease sensitive sites in Aβ(1–40) and Aβ(1–42) is a common, extended, protease-resistant region encompassing Ala21–Ala30. All nine peptide bonds in this region are substrates for various proteases used in the experiments. Eight of nine bonds are substrates for two or more proteases. This suggests that the Ala21–Ala30 region is structured.

Limited proteolysis of Aβ(21–30)

To facilitate detailed biophysical studies of the Ala21–Ala30 region of Aβ, the corresponding decapeptide, Aβ(21–30), was chemically synthesized and its protease sensitivity studied. In 25 mM ammonium acetate (pH 7.5), Aβ(21–30) was resistant to cleavage by

Table 2. *Initial cleavage sites in Aβ(1–40)*[a]

Cleavage site	Enzyme	Fragment	Observed mass	Calculated mass	Δ
Phe4–Arg5	CT	1–4	480.6	481.5	−0.5
		5–40	3867.5	3868.4	−0.9
His6–Asp7	AspN	1–6	775.2	774.8	0.4
		7–40	3574.9	3575.1	−0.2
Glu11–Val12	GluC	1–11	1326.4	1326.3	0.1
		12–40	3023.4	3023.6	−0.2
Val12–His13	HNE, PPE	1–12	1425.5	1425.5	0
		13–40	2925.4	2925.4	0
Lys16–Leu17	TR, TH	1–16	1955.8	1956.0	−0.2
		17–40	2393.7	2393.9	−0.2
Leu17–Val18	TH, CT, PPE, HNE	1–17	2069.0	2069.2	0.2
		18–40	2280.4	2280.7	−0.3
Val18–Phe19	TH, PPE, HNE	1–18	2169.1	2168.3	0.8
		19–40	2181.4	2181.6	−0.2
Phe19–Phe20	CT, TH	1–19	2315.9	2315.5	0.4
		20–40	2033.5	2034.4	−0.9
Phe20–Ala21	CT	1–20	2462.4	2462.7	−0.3
		21–40	1887.4	1887.2	0.2
Ala30–Ile31	TH	1–30	3391.4	3391.6	−0.2
		31–40	958.5	958.3	0.2
Ile31–Ile32	HNE	1–31	3504.9	3504.8	0.1
		32–40	844.6	845.1	−0.5
Ile32–Gly33	HNE	1–32	3617.8	3618.0	−0.2
		33–40	731.7	731.9	−0.2
Gly33–Leu34	TH	1–33	3675.1	3675.0	0.1
		34–40	674.4	674.9	−0.5
Met35–Val36	CT	1–35	3918.5	3919.4	−0.9
		36–40	429.9	430.5	−0.6
Val36–Gly37	HNE	1–36	4018.5	4018.5	0
		37–40	330.6	331.4	−0.8
Val39–Val40	PPE	1–39	4231.2	4231.7	−0.5
		40	N.O.	118.2	

[a] LMW Aβ(1–40) was incubated with each of seven different endoproteinases. LC/MS was performed periodically to identify fragment ions. From these data, cleavage sites and the time dependence of site-specific cleavages were determined. Initial sites of cleavage are presented here. "N.O." signifies "not observed." See Materials and Methods for experimental details.

GluC, HNE, PPE, and TR, even after extended (5 d) incubation at 25°C at an E:S ratio of 1:100 (data not shown). CT was not used because no sensitive sites exist in the decapeptide. The peptide was digested partially by AspN, yielding the fragments Ala21–Glu22 (219.0 Da, $\Delta(amu_{expected} - amu_{observed}) = -0.2$) and Asp23–Ala30 (747.5 Da, $\Delta = -0.3$). TH, whose substrate specificity includes all peptide bonds within Aβ(21–30) except Glu22–Asp23, did not digest the peptide even after prolonged incubation (4 d at a 1:1000 E:S ratio). However, under harsher digestion conditions (E:S ratio of 1:10), peptide fragmentation was observed. One hour of incubation under these conditions produced cleavages at Asp23–Val24, Gly25–Ser26, Ser26–Asn27, Lys28–Gly29, and Gly29–Ala30. The initial protease resistance of Aβ(21–30)—the same behavior exhibited by this sequence within full-length Aβ—was remarkable because such behavior is not generally observed among short peptides, which are usually unstructured and thus highly susceptible to proteolysis. Taken together with the proteolysis experiments on full-length Aβ, the data suggest that Aβ(21–30) also is structured.

Study of the protease sensitivity of the Aβ(21–30) decapeptide provided additional evidence that the protease resistance observed in this region in the full-length peptides was due to peptide folding and not to sequence. Cleavage products from seven of nine sites in the Aβ(21–30) region could be identified in the full-length peptides if alteration in time or E:S ratio was made. If the Aβ(21–30) peptide had been synthesized to determine protease specificity, then the sine qua non for substrate identification would be cleavage at specific peptide bonds. Digestion of Aβ(21–30) revealed peptide cleavage products resulting from cleavage at six of the seven peptide bonds identified in the full-length peptides. Because TH is theoretically active at all bonds in Aβ(21–30) except one, a likely explanation for the lack of detection of all possible cleavage products is that

Table 3. *Initial cleavage sites in Aβ(1–42)*[a]

Cleavage site	Enzyme	Fragment	Observed mass	Calculated mass	Δ
Phe4–Arg5	CT	1–4	N.O.	481.5	
		5–42	4051.8	4052.7	−0.9
His6–Asp7	AspN	1–6	774.8	774.8	0
		7–42	3758.9	3759.3	−0.4
Glu11–Val12	GluC	1–11	1326.4	1326.3	0.1
		12–42	3207.2	3207.8	−0.6
Val12–His13	HNE	1–12	1425.3	1425.5	−0.2
		13–42	3107.8	3108.7	−0.9
Lys16–Leu17	TR, TH	1–16	1955.3	1956.0	−0.7
		17–42	2577.7	2578.1	−0.4
Leu17–Val18	CT, PPE, HNE, TH	1–17	2069.5	2069.2	−0.3
		18–42	2464.4	2464.9	−0.5
Val18–Phe19	PPE, HNE, TH	1–18	2168.0	2168.3	−0.3
		19–42	2365.7	2365.7	−0.1
Phe19–Phe20	CT, TH	1–19	2315.0	2315.5	−0.5
		20–42	2218.6	2218.6	0
Phe20–Ala21	CT	1–20	2463.0	2462.7	−0.3
		21–42	2071.1	2071.5	−0.4
Ala30–Ile31	TH	1–30	3391.2	3391.6	−0.4
		31–42	1142.0	1142.5	−0.5
Ile31–Ile32	HNE	1–31	3504.7	3504.8	−0.1
		32–42	1028.6	1029.3	−0.7
Ile32–Gly33	HNE	1–32	3618.3	3618.0	0.3
		33–42	916.2	916.2	0
Gly33–Leu34	TH	1–33	3674.7	3675.0	−0.3
		34–42	859.5	859.1	0.4
Met35–Val36	CT	1–35	3919.5	3919.4	0.1
		36–42	614.3	614.8	−0.5
Val36–Gly37	HNE	1–36	4019.1	4018.5	0.6
		37–42	515.0	515.6	−0.6

[a] LMW Aβ(1–42) was incubated with each of seven different endoproteinases. LC/MS was performed periodically to identify fragment ions. From these data, cleavage sites and the time dependence of site-specific cleavages were determined. Initial sites of cleavage are presented here. "N.O." signifies "not observed." See Materials and Methods for experimental details.

certain of the peptide fragments were converted rapidly into amino acids that would not have been detected in our LC/MS system. We emphasize that limited proteolysis produced no cleavage of any of the nine peptide bonds in the Aβ(21–30) region of full-length Aβ(1–40) or Aβ(1–42), yet at least seven of these bonds were demonstrated to be protease substrates experimentally. This is strong evidence that sequence-specific protease resistance is not an explanation for the observed lack of cleavage within the 21–30 region of Aβ.

Solution-state NMR spectroscopy of Aβ(21–30)

Two-dimensional homonuclear NMR of Aβ(21–30)

The surprising structural stability and lack of aggregation of Aβ(21–30) suggested that the peptide would be amenable to high-resolution structural analysis using solution-state NMR. Therefore, a series of 1D and 2D NMR experiments were undertaken. The backbone amide (NH) resonances of Aβ(21–30) were resolved in one-dimensional (1D) ^{1}H NMR spectra collected on a 1-mM peptide sample in 25 mM ammonium acetate buffer (pH 6.0), at 10°C (data not shown). All of the proton resonance assignments were completed using a combination of DFQ-COSY, TOCSY, and ROESY spectra. The TOCSY spectrum of Aβ(21–30) collected using a 45-msec mixing time showed a single set of resolved resonances for each residue (data not shown). The line width of the backbone amide (NH) proton resonance of Glu22 incrementally decreased, and the peak intensity increased significantly, as the temperature was reduced from 25°C to 15°C to 10°C (data not shown). The narrow line widths of all other backbone NH proton resonances remained unchanged across the temperature range studied. In addition, although broad, the Hε–Hζ N, Hδ–Hζ N, and Hγ–Hζ N side-chain resonances of Lys28 were observed in the TOCSY spectrum suggesting that this extended side chain is stabilized or immobilized. The NH proton chemical shift dispersion was optimal at 10°C; therefore,

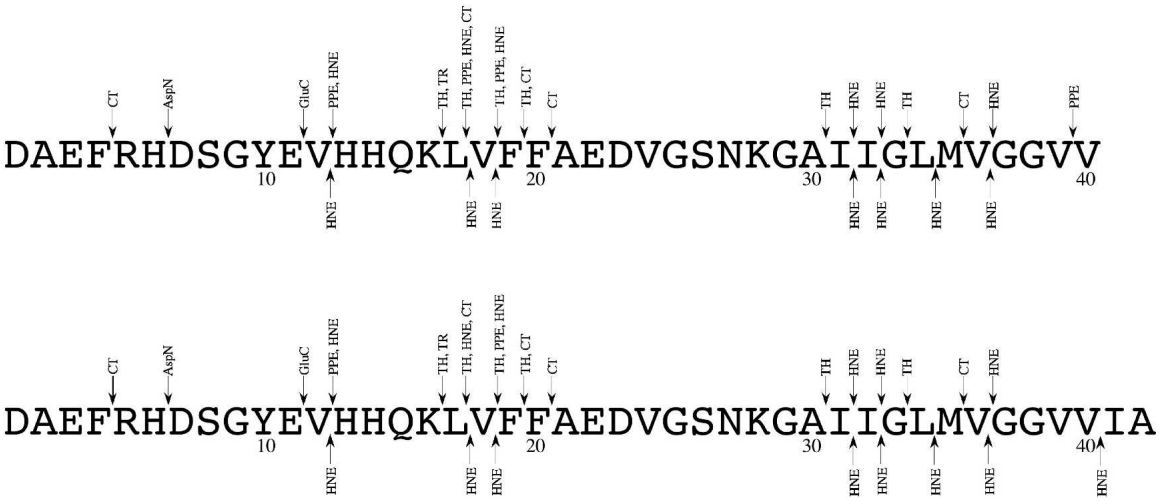

Figure 3. Summary of the locations of initial cleavage sites in Aβ(1–40) and Aβ(1–42). Initial cleavage sites are indicated by arrows followed by enzyme. Arrows below the amino acid sequence of Aβ indicate cleavage sites in the presence of 5 M Gu•HCl.

NMR data necessary for the structure determination of Aβ(21–30) were acquired at this temperature.

Amide proton exchange rates of Aβ(21–30)

Amide proton exchange rates were used to qualitatively assess hydrogen bonding in Aβ(21–30). Theoretically, hydrogen exchange rates of backbone amide protons in Aβ(21–30) in an extended, solvent-exposed conformation at 10°C and pH 6.0 should range from 0.2 to 120 min^{-1} (Bai et al. 1993). The amide proton exchange rates in Aβ(21–30) were determined experimentally using samples prepared in D_2O (data not shown). With the exception of the amide proton of Ala30, which exchanged at a rate of 0.04 min^{-1}, all of the amide proton resonance exchange rates were determined to be within the theoretical range calculated. These data indicate that the backbone of Aβ(21–30) is solvent accessible and that its structure is not stabilized by hydrogen bonding.

Two-dimensional Overhauser effect spectroscopy

2D NOESY spectra were collected with mixing times between 100 and 250 msec. Only the interresidue αH-NH($i,i + 1$) cross-peaks and select intraresidue side-chain cross-peaks were observed. This paucity of resonances is a result of the relationship between the rotational correlation (tumbling) time τ_c of a molecule and its NOE intensity (Wüthrich 1986). For Aβ(21–30), which has a molecular weight of 947 Da, the tumbling time is such that the NOE intensity approaches zero. However, this effect is experimentally overcome by collecting rotating frame Overhauser effect spectroscopy (ROESY) data. This is demonstrated for ROESY spectra of Aβ(21–30) collected at 10°C with mixing times between 100 and 400 msec (Fig. 4A). These data provided ROE resonances for the protons of Aβ(21–30) that were converted into distance measurements and used in subsequent structure calculations. In Figure 4A, an expanded NH-αH proton ("fingerprint") region of a representative ROESY spectrum shows the sequential residue αH-NH($i,i + 1$) connectivities observed throughout the peptide backbone as well as intraresidue αH-NH(i,i) cross-peaks. This spectrum is annotated with line connectivities that are drawn from the intraresidue αH-NH(i,i) cross-peak to the corresponding sequential αH-NH($i,i + 1$) cross-peak throughout the peptide sequence.

The ratios of ROE intensities for αH-NH($i,i + 1$)/αH-NH(i,i) resonances show a distinct pattern for residues involved in a β-turn-like backbone structure (Maynard et al. 1998; Griffiths-Jones et al. 1999). Specifically, for residues within the extended β-strands preceding and following the β-like turn, the ratio of αH-NH($i,i + 1$)/αH-NH(i,i) ROE intensities exceeds ~2.3. This ratio is < 1 for residues involved in the β-like turn. The ratio of αH-NH($i,i + 1$)/αH-NH(i,i) ROE intensities in the Aβ(21–30) ROESY data illustrates this trend, suggesting the presence of a β-like backbone turn within the Aβ(21–30) peptide. Glu22, Asp23, and Val24 in the amino terminal region of Aβ(21–30) exhibited an average ratio > 7.6 (range 15–3.7). Lys28 had a ratio of 3.3. The ratio decreased significantly for residues Gly25 (0.83) and Ser26 (0.46), and moderately for Asn27 (2.1), further supporting the hypothesis that Gly25 and Ser26 are involved in a β-like turn. Taken together, the observed ROE intensities for Aβ(21–30) support a turn-type conformational order in the peptide backbone localized to residues Gly25–Asn27 (Griffiths-Jones et al. 1999).

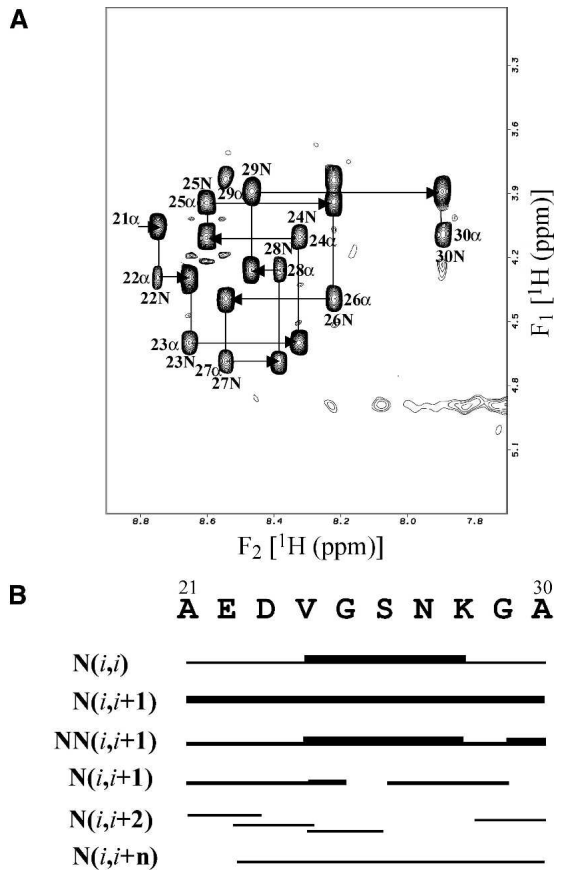

Figure 4. 2D ^{1}H ROESY NMR spectrum of Aβ(21–30). (*A*) A portion of the 2D ROESY spectrum of Aβ(21–30) in 25 mM ammonium acetate (pH 6.0), collected at 10°C with a mixing time of 300 msec. Line connectivities are illustrated for all sequential αN(*i*,*i* + 1) resonances with arrows that follow the intraresidue αN(*i*,*i*) crosspeak to its corresponding sequential αN(*i*,*i* + 1) cross-peak, and solid lines that follow the sequential αN(*i*,*i* + 1) cross-peak to its corresponding intraresidue αN cross-peak. (*B*) A summary of sequential and short- to medium-range proton connectivities from 2D ROESY data of Aβ(21–30) in 25 mM ammonium acetate (pH 6.0), collected at 10°C. Bar thickness represents the intensity of the intraresidue αN(*i*,*i*) and sequential NN(*i*,*i* + 1), αN(*i*,*i* + 1), αN(*i*,*i* + 1) proton NOE-type connectivities. All other observed ROEs are represented by lines between residues.

Spatial proton connectivities in the ROESY data of Aβ(21–30)

Elements of regular secondary structure yield distinct ROE cross-peak patterns. Following complete proton resonance assignments (Supplemental Table S1), short-, medium-, and long-range ROE interactions were defined from ROESY spectra. We examined all of the observed ROE interactions in Aβ(21–30) for recognizable sequential proton connectivity patterns typically associated with α-helices or β-sheet structure. The sequential and ROE connectivities from αH-, βH, and NH-proton resonances of one residue to a neighboring residue within the Aβ(21–30) peptide are summarized in Figure 4B. Line thickness is directly proportional to the strength of each ROE connectivity. Based upon ROE cross-peak patterns alone, no regular secondary structure element was observed in Aβ(21–30). This result, which is consistent with data from CD spectroscopy (Supplemental Fig. S8), reduces the likelihood that intramolecular hydrogen bonds, such as those that stabilize α-helices or β-sheet structures, are involved in stabilizing the Aβ(21–30) structure. Thus, the forces that stabilize the Aβ(21–30) structure in an aqueous environment likely are a combination of Coulombic, hydrophobic, and van der Waals. There are several ROE interactions between Glu22 and Lys28 which indicate the contributions of attractive electrostatic forces in stabilizing the Aβ(21–30) structure. Furthermore, the presence of ROE resonances involving the labile side-chain protons of Lys28 to Glu22 and Asp23 suggests protection of the Lys28 side chain from hydrogen exchange by the Aβ(21–30) structure, most likely through electrostatic interactions with Glu22 and Asp23. In addition, the presence of ROEs between Val24 and Lys28 reveals the contributions of side-chain–side-chain hydrophobic interactions in stabilizing the Aβ(21–30) structure. A single long-range, weak ROE between the αH proton of Glu22 and the amide proton of Ala30 provides additional evidence of a folded backbone turn. Further support for the presence of a turn is typically cross-strand backbone interactions between αH protons. Interactions of this type could not be confirmed for Aβ(21–30). αH–αH cross-peaks were not discernable off the diagonal of the spectrum due to degeneracy in the αH chemical shifts of Aβ(21–30) at all temperatures investigated. All additional ROE connectivities, other than the intraresidue and near-neighbor NH-proton correlations of the Aβ(21–30) peptide backbone, are summarized in Figure 4B.

Structure calculation of Aβ(21–30)

A total of 102 ROESY-derived distance constraints were used for iterative simulated annealing and distance geometry calculations. This produced an ensemble of 100 final structures. The ensemble of structures displays a main chain turn involving Val24, Gly25, Ser26, and Asn27; a relatively ordered, extended, amino terminal strand; and a carboxyl terminus that adopts two possible conformations (family I or family II) (Supplemental Fig. S9). The final ensemble of Aβ(21–30) structures possesses no distance violations >0.3 Å, indicating that the conformers within each family satisfy the set of distance constraints.

Solution structure of Aβ(21–30)

The geometrical averaged structure for Aβ(21–30) family I and family II conformers was determined and

energy-minimized (Fig. 5). Average root-mean-squared deviation (RMSD) values following superimposition of the backbone heavy atoms of each structure in the respective ensembles with the geometric average reflect the qualities of the two families of structures that were determined (Supplemental Table S2). For the backbone heavy atoms Glu22–Lys28, the RMSD was 0.997 Å for family I and 1.093 Å for family II. The divergence in the two Aβ(21–30) conformers occurs within the backbone atoms of Lys28, which orient the side chain of Lys28 toward the back (family I) or the front (family II) of the structure. Attractive side-chain contacts between Glu22 and Lys28 in family I, and between Asp23 and Lys28 in family II, contribute stabilizing Coulombic forces to the convergent turn structure in Aβ(21–30). These electrostatic interactions are spatially distant (> 5 Å) and therefore cannot be considered salt bridges (Marqusee and Baldwin 1987), defined here as two hydrogen-bonded atoms of opposite charge within 3.5 Å of each other (Marqusee and Baldwin 1987). In both families, experimentally determined ROEs support the presence of potential hydrophobic contacts between the side chains of Val24 and Lys28. These interactions also contribute to stabilizing the convergent turn structure.

Angular order parameter (S^2) calculations for Aβ(21–30)

The angular order parameter S^2, calculated using DGII software (Insight II), is related to the standard deviation and precision of the dihedral angle and is used to characterize the torsion angle space spread within an ensemble of structures. The upper limit ($S^2 = 1$) defines a precisely determined dihedral angle, whereas the lower limit ($S^2 = 0$) identifies a random angle distribution about a given dihedral angle. For regions of a protein that are well defined, the backbone angular order parameters for ϕ and ψ will show greater precision and angle definition ($S^2 = 1$). We used ϕ and ψ angular order parameters to compare the Aβ(21–30) structures and to assess the contributions of the NMR-derived distance constraints on the structural convergence and quality of the structures calculated (Supplemental Fig. S10). The per-residue angular order parameters determined for each of the two families calculated with our NMR-derived distance restraints are significantly higher than those calculated for the ensemble of Aβ(21–30) structures generated without NMR-derived distance restraint data. In addition, the ϕ and ψ angular order parameters for family I are higher, on average, than those measured for family II. Specifically, the angular order parameters are highest for residues Asp23 through Lys28 in family I, whereas the same region is less ordered in family II. The ϕ and ψ angular order parameters for the residues involved in the turn, Val24, Gly25, Ser26, and Asn27, approach 1 (complete order). However, the per-residue order parameter decreases for the carboxy terminal residues Gly29 and Ala30, which is a consequence of a reduced number of NMR constraints per residue and is a phenomenon characteristic of many NMR structures with "frayed" peptide termini.

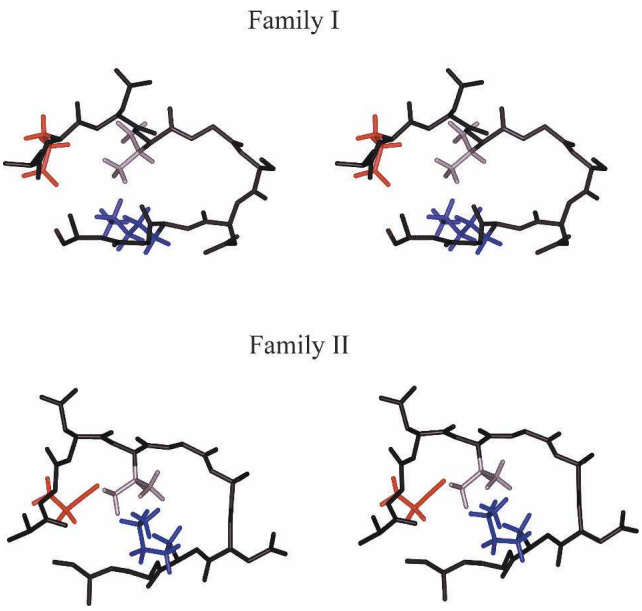

Figure 5. Final mean structures for the Aβ(21–30) conformers. The geometric average structure for each family of the Aβ(21–30) structures was determined using Analysis (InsightII) and minimized using Discover (InsightII). The entire backbone (black) and all residue side chains are shown. The side chains of residues Glu22, Val24, and Lys28, are colored red, gray, and blue, respectively.

Assembly state of Aβ(21–30)

The NMR data are consistent with results of CD experiments performed under similar conditions that suggested that the conformation of Aβ(21–30) is an intrinsic property of the monomer and is not linked to monomer self-association. The spectral linewidths of the ^{1}H resonances were narrow and representative of a small peptide tumbling with a correlation time $\tau_c \approx 0.5$ nsec, an estimate based on the size of Aβ(21–30). No temperature dependence of the ^{1}H resonance linewidths was observed, supporting the maintenance of a monomer over the temperature range studied. Furthermore, NOESY experiments using mixing times of 200–400 msec displayed a paucity of NOE cross-peaks at 500 MHz, a phenomenon common with small peptides (500–1500 Da). An NOE null effect is exhibited by peptides in this molecular mass range because the product $\omega_0\tau_c \approx 1$ (where ω_0 is the Larmor frequency) (Wüthrich 1986). To circumvent this null effect, data can be collected at very low temperatures, which increases the solvent viscosity and decreases the tumbling rate. However, this approach results in substantial ^{1}H line broadening and poor solvent suppression,

which ultimately decreases signal-to-noise ratios. For this reason, we used the ROESY approach, which eliminates τ_c dependence, and thus molecular mass dependence, from the data collected. The positive ROESY signal, which is independent of the molecular mass, allows for the detection of dipolar couplings between nuclei in small molecules that might not otherwise be observed in a NOESY spectrum. In addition to the monomer-like tumbling properties of Aβ(21–30), we observed rapid ^{1}H exchange when the bulk solvent was 99.996% D_2O. Aggregated proteins display protection from exchange. Taken together, these data support the conclusion that the NMR data derive from monomeric Aβ(21–30).

Discussion

The data presented here are consistent with the postulation that one of the initial events in pathologic Aβ monomer folding is an intramolecular nucleation event in which the Val24–Lys28 region forms an unusual turn conformation centered at Gly25–Asn27 (Fig. 6). It is possible that a Val24–Lys28 five-residue turn may result from (i,i + 1) double turns (Hutchinson and Thornton 1994), which consist of five residues such that residues 1–4 (Val24–Gly25–Ser26–Asn27) and residues 2–5 (Gly25–Ser26–Asn27–Lys28) form turns. The central residues in the Val-Gly-Ser-Asn and Gly-Ser-Asn-Lys turns (Gly-Ser and Ser-Asn, respectively) have high overall positional potential to form the central residues of β-turns (Hutchinson and Thornton 1994). Multiple elements thus may contribute to the formation and stabilization of the turn in Aβ monomer, including: (1) the intrinsic propensity of Val-Gly-Ser-Asn and Gly-Ser-Asn-Lys sequences to form β-turns (Hutchinson and Thornton 1994); (2) hydrophobic interactions between Val24 and Lys28 side chains; and (3) long-range Coulombic interaction between Lys28 and either Glu22 or Asp23. The existence of two conformational families may reflect competition between the carboxylate anions of these two latter amino acids for the NH_3^+ group of Lys28.

The observations of a folding nucleus within the Ala21–Ala30 region of full-length Aβ and a homologous structure in the isolated Aβ(21–30) decapeptide are consistent with previous work showing that peptide fragments encompassing the folding nuclei of globular proteins, by themselves, are structured (Neira and Fersht 1996). Furthermore, the structures found in the folding nuclei are similar to those found in the holoproteins (Neira and Fersht 1996). Our data are consistent with the Aβ folding nucleus appearing in the monomer form of the peptide. The data reported here, and by others (Kheterpal et al. 2003), demonstrates that nonmonomer forms of Aβ, including oligomers, protofibrils, and fibrils, show backbone peptide-bond protection. Aβ amyloid formation, and amyloid formation by other proteins, is thought to be driven to a significant degree by hydrophobic interactions among peptide segments that are solvent-exposed in the partially unfolded state (Dobson 1999). We observed that hydrophobic regions in Aβ(1–40), including the CHC and the C terminus, were accessible to proteolysis (Fig. 3) and therefore not involved either in intra- or intermolecular folding interactions. Previously, we demonstrated that both LMW Aβ(1–40) and Aβ(1–42) exist in equilibria among monomers and low-order (low n) oligomers: n = 2–4 for Aβ(1–40) and n = 5,6 for Aβ(1–42) (Bitan et al. 2003a). These equilibria are extremely rapid, establishing themselves from the pure monomer state with time constants << 1 min (Bitan et al. 2003a). We also showed that some structural order exists in chemically-stabilized oligomers (Bitan et al. 2003a). Hydrogen exchange experiments have confirmed that protection factors in oligomers differ significantly from monomers (Kheterpal et al. 2003). A consideration of these published data, and the results reported here, suggests that a simple and logical explanation for our data is that proteolysis revealed peptide bond exposure primarily in the monomer state and that this state, following Le Châtelier's principle (Le Châtelier 1884), was rapidly repopulated by disassembly of low-order oligomers during the digestion procedure.

We note that the Val39–Ala42 region in LMW Aβ(1–42) is protease-resistant in the absence of denaturant (Fig. 3). This resistance in the monomer state requires structure, which may involve Gly–Gly turns (Grant et al. 2000; Gibbs et al. 2002). β-Helix models of fibrils formed by full-length Aβ (Lazo and Downing 1998) and Aβ(34–42) (Lazo and Downing 1999) contain Gly37–Gly38 turns.

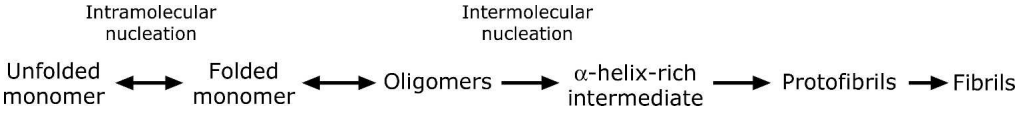

Figure 6. Aβ folding and assembly. Multiple nucleation processes occur during Aβ fibril assembly. "Intramolecular nucleation" refers to the structural organization of an initially unfolded monomer. The resulting partially folded conformers oligomerize in an alloform-specific manner to produce the distinct oligomer distributions displayed by Aβ40 and Aβ42 (Bitan et al. 2003a). These oligomers serve to nucleate subsequent higher order assembly reactions. The conformational transformations associated with oligomer formation thus are referred to as "intermolecular nucleation."

Importantly, in silico studies of Aβ monomer folding have shown that a Gly37–Gly38 turn forms in Aβ(1–42) but not in Aβ(1–40) (Urbanc et al. 2004).

Our work offers a mechanistic explanation for the effects of disease-associated amino acid substitutions clustered in the Ala21–Ala30 region of Aβ. Five such substitutions have been reported, all of which are found between Ala21 and Asp23. The mutations giving rise to the substitutions are named after the ethnicities of the kindreds in which they were identified and include the Flemish (Ala21→Gly) (Cras et al. 1998), Arctic (Glu22→Gly) (Kamino et al. 1992; Nilsberth et al. 2001), Dutch (Glu22→Gln) (Levy et al. 1990), Italian (Glu22→Lys) (Bugiani et al. 1998), and Iowa (Asp23→Asn) (Grabowski et al. 2001) mutations. The existence of long-range stabilizing Coulombic interactions between Glu22/Asp23 and Lys28, and the involvement of the aminobutyl side chain of Lys28 in hydrophobic interactions, offer an explanation for how these AD- and cerebral amyloid angiopathy-linked amino acid substitutions cause pathology—they alter the structure or stability of the folding nucleus. How these alterations affect the biophysical and biological properties of the peptide segment defining the folding nucleus is difficult to determine pre facto. As with any mutation in a protein structural gene, we would predict a priori that substitutions could enhance, inhibit, or have no effect on peptide segment-specific properties. In practice, substitutions in the Aβ(21–23) region have been shown to cause aberrant AβPP processing (Aβ anabolism) (Hardy 1997), inhibition of Aβ degradation and clearance (Aβ catabolism) (Tsubuki et al. 2003), increased peptide neurotoxicity (Melchor et al. 2000), and changes in Aβ assembly kinetics or pathway. For example, the Arctic mutation leads to enhanced Aβ protofibril formation but decreased overall Aβ production (Nilsberth et al. 2001). All three Glu22 substitutions lead to enhanced fibril assembly on the surface of human cerebrovascular smooth muscle cells, where amyloid is deposited in cerebral amyloid angiopathy (Melchor et al. 2000).

Conceptually, the biophysical basis of mutation-induced, accelerated Aβ self-association has been thought to be the enhanced ability of the altered amino acid side chain to incorporate into pathologic structures. The data presented here provide deeper mechanistic insights into the assembly process and suggest alternative explanations to explain mutant phenotypes. Specifically, primary structure changes within the Ala21–Ala30 decapeptide segment alter pathways of nucleation. These alterations can either be quantitative (kinetic) or qualitative (altering pathway choice). Substitutions at Glu22 or Asp23 would affect long-range interactions of these amino acids with Lys28, changing the propensity of the Aβ monomer to populate conformational family I or II. The Italian, Dutch, and Arctic mutations, for example, would destabilize the Coulombic Glu22:Lys28 interaction, shifting the folding pathway away from family I toward family II. If fibril formation from family II conformers were more favorable energetically than from family I conformers, disruption of Glu22:Lys28 interactions within the folding nucleus could produce the counterintuitive result of increased fibril formation. Results from recent discrete molecular dynamics simulations of Aβ(21–30) folding support this postulation (Borreguero et al. 2005). These simulations show that electrostatic interactions between Asp23 and Lys28 are favored over those involving Glu22 and Lys28 in conformers with a propensity for fibril formation. In fact, experimental studies have shown that an engineered lactam bridge between Asp23 and Lys28 increases the Aβ(1–40) fibrillogenesis rate by ≈1000-fold (Sciarretta et al. 2005). In addition to those substitutions enhancing nucleation, certain substitutions might inhibit monomer nucleation. These latter mutations would be nonpathogenic, and therefore it is unlikely they would be identified clinically using strategies designed to recognize pathologic phenotypes.

Wurth et al. (2002) have used an unbiased genetic approach to identify amino acid substitutions in Aβ(1–42) that reduced the aggregation of Aβ(1–42)-green fluorescent protein (GFP) fusion proteins in *Escherichia coli*. This approach revealed six strains in which substitutions in the Aβ(21–30) region occurred: GM71, Glu22→Gln, Ala30→Pro; GM57, Ser26→Phe; GM13, Val24→Gly; GM11 and GM16, Val24→Ala; and GM9, Ser26→Pro. Unfortunately, all of these strains expressed fusion proteins in which amino acid substitutions also occurred outside the Aβ(21–30) region, complicating structure–activity correlation. It is provocative, however, that the mutations that were observed involved residues predicted by our structural model to have significant influence on Aβ folding, including Glu22 (Coulombic interactions), Val24 (hydrophobic interactions), and Ser26 (turn formation). Williams et al. (2004) used a different approach, scanning proline mutagenesis, to study secondary structure within fibrils formed by Aβ(1–40) and to derive a model of the Aβ(1–40) protofilament. This model differs from those derived by solid-state NMR (Petkova et al. 2002), especially with respect to the location of turns. Rather than predict a turn in the 25–29 region, Williams et al. predict two turns, one centered at Glu22–Asp23 and the other centered at Gly29–Ala30. Additional studies will be required to reconcile these differing models of fibril structure. Our data are relevant to the earliest folding events in Aβ self-assembly and suggest that relatively minor rearrangement is necessary to produce fibrils arranged as suggested by Petkova et al. (2002). However, our model does not exclude the possibility of more substantial rearrangement, as would be required to satisfy the model of Williams et al. (2004).

We have focused here on full-length Aβ proteins and the Aβ(21–30) peptide. Zhang et al. (2000) examined the structure of an Aβ fragment intermediate in size, Aβ(10–35). This peptide has been an object of study because it has been found to be "plaque competent," i.e., it provides a source of monomers for elongation of pre-existent fibrils (Lee et al. 1995). Based on distance constraints from NOESY data, Zhang et al. derived two equally probable families of structures for Aβ(10–35). The key feature of these families was a collapsed coil structure formed by the CHC, accompanied by "a series of loops and turns condensed about the CHC foundation." To assess any similarities or differences among the structures derived by Zhang et al. and those presented here, we superimposed the backbones of our families I and II on their respective regions within Aβ(10–35) (data not shown). We found that the superimposition of the backbone of family I from Asp23 to Lys28 with that of Aβ(10–35) (PDB ID 1HZ3) produced excellent agreement, particularly along the SN sequence.

We are aware of one solution-state NMR study examining full-length, unmodified Aβ in cosolvent-free, aqueous solution (Hou et al. 2004). Using Aβ(1–40) and Aβ(1–42) in phosphate-buffered solution (pH 7.2), Hou et al. (2004) concluded that both proteins contain turn- or bend-like structures at Asp7–Glu11 and Phe20–Ser26. The only two regions of full-length Aβ that we found contained four or more contiguous protease-resistant peptide bonds were Asp7–Glu11 and Ala21–Ala30. The former region matches precisely that defined by Hou et al. The region Phe20–Ser26 differs somewhat from, but is largely contained within, the Ala21–Ala30 segment we defined. The lack of perfect correspondence between the two data sets may be related to differing experimental conditions. To delay β-sheet formation, Hou et al. performed their experiments at 5°C. At this temperature, medium-range NOEs throughout the Phe20–Ala30 region were observed and it was speculated that the region exists as an ensemble of rapidly interconverting random structures with kink- or bend-like propensities (Hou et al. 2004). At 25°C, the temperature used in our limited proteolysis studies, it is possible that a turn region similar to family I or II might be populated more frequently.

One prediction of the monomer nucleation model we have proposed is that the nucleation center should be present in fibrils, the end-stage assemblies of Aβ self-association. Although a complete three-dimensional structure of Aβ fibrils has not yet been determined (Tycko 2004), evidence from a number of groups supports the existence of a turn or bend structure. Early studies on Aβ(10–43) fibrils containing disulfide bridges suggested that a β-turn was present from Ser26 to Gly29 (Hilbich et al. 1991). More recently, supported by solid-state NMR data, Petkova et al. (2002) proposed a model for Aβ(1–40) fibrils incorporating a bend region at Gly25–Gly29. This structure would bring the CHC and C terminus into contact, allowing hydrophobic side-chain interactions, an obligate step in fibril formation (Petkova et al. 2002). Our results show that rudimentary forms of the turn or bend structure found in fibril-associated β-sheets are already present in Aβ monomer and are metastable in isolation. An interesting outcome of recent molecular dynamics simulations (Ma and Nussinov 2002) and modeling based on NMR data (Petkova et al. 2002) is the suggestion that the turn or bend region in Aβ fibrils is stabilized by an intramolecular salt bridge involving Asp23 and Lys28. The distance between C_γ of Asp23 and N_ζ of Lys28 in the two families of structures (13 Å in family I and 9 Å in family II) would produce a much weaker Coulombic interaction than that associated with the ~4 Å bond distance in fibrils (Petkova et al. 2002). In addition, in our model, Val24 forms hydrophobic contacts with the side chain of Lys28 and is buried within the core of the turn structure. However, Val24 is solvent-exposed in the model of Aβ(1–40) fibrils proposed by Petkova et al. (2002). This suggests that partial unfolding or rearrangement of the folding nucleus of Aβ monomer occurs during fibril assembly. This rearrangement could be driven by intermolecular interactions, resulting in the formation of an α-helical intermediate (Kirkitadze et al. 2001), which subsequently leads to protofibrils and fibrils (Fig. 6). Experimental studies of fibril assembly thermodynamics, and theoretical treatments thereof, both are consistent with this notion (Kusumoto et al. 1998; Esler et al. 2000a,b; Massi and Straub 2001).

Materials and methods

Peptides and enzymes

Aβ(1–40) and Aβ(1–42) were synthesized using 9-fluorenylmethoxycarbonyl chemistry, purified by RP-HPLC, and characterized by electrospray ionization mass spectrometry and amino acid analysis, as described (Lomakin et al. 1996). Chymotrypsin (CT), endoproteinase Asp-N (AspN), endoproteinase Glu-C (GluC), porcine pancreatic elastase (PPE), and trypsin (TR) were purchased from Roche. Thermolysin (TH) was purchased from Sigma. Human neutrophil elastase (HNE) was purchased from Calbiochem.

Preparation of LMW Aβ(1–40) and Aβ(1–42)

Aggregate-free preparations of Aβ, termed LMW Aβ (Walsh et al. 1999), were prepared in 25 mM ammonium acetate (pH 7.5), by filtration through a 10-kDa molecular weight cutoff Microcon YM-10 centrifugal filter device (Amicon Bioseparations), essentially as described (Fezoui et al. 2000). In some experiments, the buffer contained 5 M ultrapure (≥99.5%) guanidine hydrochloride (Gu•HCl; Sigma). Peptide

concentrations were determined by UV absorbance at 275 nm using an extinction coefficient $\varepsilon_{275} = 1390\ M^{-1}\ cm^{-1}$ (for buffer alone) or $\varepsilon_{275} = 1450\ M^{-1}\ cm^{-1}$ (for Gu•HCl-containing buffer).

Circular dichroism (CD) spectroscopy

CD spectra of Aβ(1–40), Aβ(1–42), and Aβ(21–30) were acquired at 25°C immediately after peptide preparation using an Aviv 62A DS spectropolarimeter (Aviv Associates) over a wavelength range of 260 to 195 nm. Stoppered 1-mm pathlength quartz cells (Starna Cells) were used. Readings were recorded every 1 nm with an averaging time of 5–10 sec and a bandwidth of 1 nm. Mean residue ellipticity (Θ) was determined according to the equation $\Theta = \Theta_{Obs} \bullet MRW/(10 \bullet l \bullet c)$; where Θ_{Obs} is observed ellipticity (degrees), MRW is mean residue weight of the peptide (peptide molecular weight divided by the number of residues), c is peptide concentration (g/L), and l is optical path length (cm). Peptide concentrations were determined by quantitative amino acid analysis. Spectral deconvolution was performed using CDPro (Sreerama and Woody 2000).

Limited proteolysis

Enzymatic digestions of LMW Aβ were performed in 25 mM ammonium acetate buffer (pH 7.5). Five M guanidine hydrochloride (Gu•HCl) was included in some experiments. Enzyme:substrate (E:S) ratios were adjusted following determination of peptide concentration by UV absorbance. Proteolysis was done at 25°C using E:S ratios of 1:10, 1:100, 1:500, or 1:1000. Aliquots of each digestion were removed periodically and the reactions quenched by acidification with 1% (v/v) trifluoroacetic (TFA) acid in water.

Liquid chromatography/mass spectrometry (LC/MS)

Peptide fractionation and mass spectrometry were performed on an LCQDECA LC/MS system from ThermoFinnigan (San Jose, CA). This system consists of a Surveyor HPLC system interfaced to an LCQDECA electrospray ionization/ion trap mass spectrometer. The digests were fractionated on 150 mm × 1.0 mm, 5-μm particle size C18, C4, or diphenyl columns (Grace Vydac). Solvent A was 0.1% (v/v) glacial acetic acid and 0.02% (v/v) TFA in H_2O. Solvent B was 90% (v/v) acetonitrile in H_2O. The elution program comprised a 5-min post-injection 0% B isocratic stage, followed by a 25-min duration 0%→30% B gradient and a 30-min 30%→50% B gradient. The flow rate was maintained at 100 μL/min. Elution was monitored by UV absorbance using a Surveyor photodiode array detector with two-channel recording (214 nm and 259 nm). Effluent from the detector was introduced directly into the source of the LCQDECA. The spray voltage was 4.5 kV and the capillary temperature was 250°C. Nitrogen was used as sheath and auxiliary gas. Mass spectra were obtained in positive ion mode. Collisions for data-dependent MS^2 experiments were carried out with an isolation window of 2.0 units, a normalized collision energy of 40%, and an activation time of 30 msec. Isobaric peptides were unambiguously identified by analysis of their characteristic fragmentation patterns.

Three-dimensional structure determination of Aβ(21–30) from NMR data

One-dimensional (1D) ^1H and two-dimensional (2D) ^1H-^1H (homonuclear) NMR data of the Aβ(21–30) peptide were recorded over at temperature range of 10°–25°C on a 500 MHz Varian Unity INOVA spectrometer with a proton frequency of 499.695 MHz. Samples contained 1 mM synthetic Aβ(21–30) peptide dissolved in either 25 mM ammonium acetate in H_2O:D_2O (9:1, v/v) (pH 6.0), or 25 mM d_4-acetate in 99.996% D_2O (Cambridge Isotope Laboratories). The carrier frequency was set to the water resonance, which was suppressed using presaturation during the preacquisition delay.

Two-dimensional total correlation spectroscopy (TOCSY) spectra were recorded with a mixing time of 45 msec using the MLEV-17 spin-lock sequence (Bax and Davis 1985). A total of 4096 real data points were acquired in t_2 and 256 time-proportional phase increments (TPPI) were implemented in t_1 with a spectral width of 8000 Hz in the F_2 dimension. A total of 192 summed transients were collected with a relaxation delay of 1.1 sec. Spectra were processed offline with Gaussian and sine bell functions for apodization in t_2 and a shifted sine bell function in t_1 using VNMR software processing (Varian, Inc.). All data were zero filled to 4K by 2K real matrices. A 2D double-quantum filtered correlation spectroscopy (DQF-COSY) spectrum was acquired with 4096 real data points in t_2 and 640 TPPI were implemented in t_1 with a spectral width of 8000 Hz in the F_2 dimension. A total of 96 summed transients were collected for potential measurement of $^3J_{NH\alpha}$ spin–spin coupling constants. Two-dimensional rotating frame Overhauser enhancement spectroscopy (ROESY) spectra were recorded with mixing times of 100, 200, 300, and 400 msec (Hwang and Shaka 1992). A total of 4096 real data points were acquired in t_2 and 256 TPPI were implemented in t_1 with a spectral width of 8000 Hz in the F_2 dimension. A total of 128 summed transients were collected with a relaxation delay of 1.1 sec. Additional ROESY data were acquired with samples of Aβ(21–30) prepared in d_4-acetate in 99.996% D_2O in order to complete the assignments of resonances located near the residual water peak. These data also permitted the detection of weak ROESY cross-peaks that are adversely attenuated at high presaturation power levels.

All proton resonance spin-system assignments of Aβ(21–30) were completed using a combination of DFQ-COSY and TOCSY experiments, which identify ^1H-^1H through-bond connectivities. ROESY experimental data provided sequence-specific assignments and sequential $d_{\alpha N}$, $d_{\beta N}$, and d_{NN} connectivities. ROESY cross-peak intensities were classified as strong, medium, or weak and converted to distance restraint upper bounds of 2.5, 3.5, and 5.0 Å, respectively (Roberts 1993). Scalar reference peaks were chosen from nonoverlapped NH-αH ROESY peaks and set to 2.6 Å distances for calibration of the entire set of distance restraints (Wüthrich 1986). Nonstereospecifically assigned atoms were treated as pseudo-atoms and assigned correction distances (Wüthrich 1986).

The three-dimensional structure of Aβ(21–30) was determined from a total of 102 distance restraints (56 intraresidue, 46 interresidue, 35 sequential, 10 medium range, and 1 long range) which were entered into the distance geometry program, DGII (CVFF force field parameters) of InsightII (Accelrys). These data were used to generate a family of 100 structures using a combination of distance geometry and simulated annealing (Havel 1991). Two unique geometric families were determined for Aβ(21–30). A convergent ensemble of

25 structures possessing the least RMSD from the mean structure of each ensemble was used to represent each geometric family. The average structure for each ensemble was determined using the Analysis program of InsightII (Accelrys) and minimized using a steepest descents protocol within the Discover program of InsightII. The quality of these data and convergence within each family was determined using average RMSD values that were derived following the superimposition of backbone heavy atoms of each of the 25 structures with the average structure (Supplemental Table S2). To confirm that the Aβ(21–30) structures were dependent on the incorporation of distance restraints derived from NMR data and were not an empirical result of the peptide sequence, the structure of Aβ(21–30) also was determined using the protocol detailed previously but without including any distance restraints. A family of 100 structures was generated using the same simulated annealing protocol as used in the structure calculations for Aβ(21–30) using distance restraints from NMR data.

Electronic supplemental material

Results of limited proteolysis of Aβ(1–40) and Aβ(1–42) by chymotrypsin, endoproteinase Asp-N, endoproteinase Glu-C, human neutrophil elastase, porcine pancreatic elastase, and trypsin, and of Aβ(1–42) by thermolysin, are presented. CD spectroscopy of Aβ(21–30), superimpositions of 25 calculated backbone structures for each of two different families of Aβ(21–30) conformers, angular order parameter analyses of the Aβ(21–30) structure, and tables showing the ^{1}H chemical shifts and structural statistics of Aβ(21–30) also are included.

Acknowledgments

This work was supported by grants NS38328 (and a Minority Research Supplement thereto), NS44147, and AG18921 from the NIH (D.B.T.) and by the Foundation for Neurologic Diseases (D.B.T.).

References

Bai, Y., Milne, J.S., Mayne, L., and Englander, S.W. 1993. Primary structure effects on peptide group hydrogen exchange. *Proteins* **17:** 75–86.

Barrow, C.J., Yasuda, A., Kenny, P.T.M., and Zagorski, M. 1992. Solution conformations and aggregational properties of synthetic amyloid β-peptides of Alzheimer's disease. *J. Mol. Biol.* **225:** 1075–1093.

Bax, A. and Davis, D.G. 1985. MLEV-17-based two-dimensional homonuclear magnetization transfer spectroscopy. *J. Magn. Reson.* **65:** 355–360.

Benzinger, T.L.S., Gregory, D.M., Burkoth, T.S., Miller-Auer, H., Lynn, D.G., Botto, R.E., and Meredith, S.C. 2000. Two-dimensional structure of β-amyloid(10–35) fibrils. *Biochemistry* **39:** 3491–3499.

Bitan, G., Lomakin, A., and Teplow, D.B. 2001. Amyloid β-protein oligomerization: Prenucleation interactions revealed by photo-induced cross-linking of unmodified proteins. *J. Biol. Chem.* **276:** 35176–35184.

Bitan, G., Kirkitadze, M.D., Lomakin, A., Vollers, S.S., Benedek, G.B., and Teplow, D.B. 2003a. Amyloid β-protein (Aβ) assembly: Aβ40 and Aβ42 oligomerize through distinct pathways. *Proc. Natl. Acad. Sci.* **100:** 330–335.

Bitan, G., Tarus, B., Vollers, S.S., Lashuel, H.A., Condron, M.M., Straub, J.E., and Teplow, D.B. 2003b. A molecular switch in amyloid assembly: Met^{35} and amyloid β-protein oligomerization. *J. Am. Chem. Soc.* **125:** 15359–15365.

Borreguero, J.M., Urbanc, B., Lazo, N.D., Buldyrev, S.V., Teplow, D.B., and Stanley, H.E. 2005. Folding events in the 21–30 region of amyloid β-protein (Aβ) studied in silico. *Proc. Natl. Acad. Sci.* (in press).

Bugiani, O., Padovani, A., Magoni, M., Andora, G., Sgarzi, M., Savoiardo, M., Bizzi, A., Giaccone, G., Rossi, G., and Tagliavini, F. 1998. An Italian type of HCHWA. *Neurobiol. Aging* **19:** S238.

Butterfield, D.A. 2002. Amyloid β-peptide (1–42)-induced oxidative stress and neurotoxicity: Implications for neurodegeneration in Alzheimer's disease brain. *Free Radic. Res.* **36:** 1307–1313.

Coles, M., Bicknell, W., Watson, A.A., Fairlie, D.P., and Craik, D.J. 1998. Solution structure of amyloid β-peptide(1–40) in a water–micelle environment—Is the membrane-spanning domain where we think it is? *Biochemistry* **37:** 11064–11077.

Cras, P., van Harskamp, F., Hendriks, L., Ceuterick, C., van Duijn, C.M., Stefanko, S.Z., Hofman, A., Kros, J.M., Van Broeckhoven, C., and Martin, J.J. 1998. Presenile Alzheimer dementia characterized by amyloid angiopathy and large amyloid core type senile plaques in the APP 692Ala → Gly mutation. *Acta Neuropathol. (Berl).* **96:** 253–260.

Dobson, C.M. 1999. Protein misfolding, evolution and disease. *Trends Biochem. Sci.* **24:** 329–332.

Esler, W.P., Felix, A.M., Stimson, E.R., Lachenmann, M.J., Ghilardi, J.R., Lu, Y.A., Vinters, H.V., Mantyh, P.W., Lee, J.P., and Maggio, J.E. 2000a. Activation barriers to structural transition determine deposition rates of Alzheimer's disease Aβ amyloid. *J. Struct. Biol.* **130:** 174–183.

Esler, W.P., Stimson, E.R., Jennings, J.M., Vinters, H.V., Ghilardi, J.R., Lee, J.P., Mantyh, P.W., and Maggio, J.E. 2000b. Alzheimer's disease amyloid propagation by a template-dependent dock-lock mechanism. *Biochemistry* **39:** 6288–6295.

Fezoui, Y., Hartley, D.M., Harper, J.D., Khurana, R., Walsh, D.M., Condron, M.M., Selkoe, D.J., Lansbury, P.T., Fink, A.L., and Teplow, D.B. 2000. An improved method of preparing the amyloid β-protein for fibrillogenesis and neurotoxicity experiments. *Amyloid* **7:** 166–178.

Fontana, A., Polverino de Laureto, P., De Filippis, V., Scaramella, E., and Zambonin, M. 1997. Probing the partly folded states of proteins by limited proteolysis. *Fold. Des.* **2:** R17–R26.

George, A.R. and Howlett, D.R. 1999. Computationally derived structural models of the β-amyloid found in Alzheimer's disease plaques and the interaction with possible aggregation inhibitors. *Biopolymers* **50:** 733–741.

Gibbs, A.C., Bjorndahl, T.C., Hodges, R.S., and Wishart, D.S. 2002. Probing the structural determinants of type II′ β-turn formation in peptides and proteins. *J. Am. Chem. Soc.* **124:** 1203–1213.

Gorevic, P.D., Castaño, E.M., Sarma, R., and Frangione, B. 1987. Ten to fourteen residue peptides of Alzheimer's disease protein are sufficient for amyloid fibril formation and its characteristic X-ray diffraction pattern. *Biochem. Biophys. Res. Commun.* **147:** 854–862.

Grabowski, T.J., Cho, H.S., Vonsattel, J.P.G., Rebeck, G.W., and Greenberg, S.M. 2001. Novel amyloid precursor protein mutation in an Iowa family with dementia and severe cerebral amyloid angiopathy. *Ann. Neurol.* **49:** 697–705.

Grant, G.A., Xu, X.L., and Hu, Z. 2000. Role of an interdomain Gly–Gly sequence at the regulatory-substrate domain interface in the regulation of *Escherichia coli*. D-3-phosphoglycerate dehydrogenase. *Biochemistry* **39:** 7316–7319.

Griffiths-Jones, S.R., Maynard, A.J., and Searle, M.S. 1999. Dissecting the stability of a β-hairpin peptide that folds in water: NMR and molecular dynamics analysis of the β-turn and β-strand contributions to folding. *J. Mol. Biol.* **292:** 1051–1069.

Gursky, O. and Aleshkov, S. 2000. Temperature-dependent β-sheet formation in β-amyloid Aβ(1–40) peptide in water: Uncoupling β-structure folding from aggregation. *Biochim. Biophys. Acta* **1476:** 93–102.

Haass, C. and Steiner, H. 2001. Protofibrils, the unifying toxic molecule of neurodegenerative disorders? *Nat. Neurosci.* **4:** 859–860.

Haass, C., Schlossmacher, M.G., Hung, A.Y., Vigo-Pelfrey, C., Mellon, A., Ostaszewski, B.L., Lieberburg, I., Koo, E.H., Schenk, D., Teplow, D.B., et al. 1992. Amyloid β-peptide is produced by cultured cells during normal metabolism. *Nature* **359:** 322–325.

Hardy, J. 1997. The Alzheimer family of diseases—Many etiologies, one pathogenesis. *Proc. Natl. Acad. Sci.* **94:** 2095–2097.

Hardy, J. and Allsop, D. 1991. Amyloid deposition as the central event in the aetiology of Alzheimer's disease. *Trends Pharmacol.* **12:** 383–388.

Harper, J.D., Wong, S.S., Lieber, C.M., and Lansbury, P.T. 1997. Observation of metastable Aβ amyloid protofibrils by atomic force microscopy. *Chem. Biol.* **4:** 119–125.

Hartley, D.M., Walsh, D.M., Ye, C.P.P., Diehl, T., Vasquez, S., Vassilev, P.M., Teplow, D.B., and Selkoe, D.J. 1999. Protofibrillar intermediates of amyloid β-protein induce acute electrophysiological changes and progressive neurotoxicity in cortical neurons. *J. Neurosci.* **19:** 8876–8884.

Havel, T.F. 1991. An evaluation of computational strategies for use in the determination of protein structure from distance constraints obtained by nuclear magnetic resonance. *Prog. Biophys. Mol. Biol.* **56:** 43–78.

Hendriks, L. and Vanbroeckhoven, C. 1996. The βA4 amyloid precursor protein gene and Alzheimer's disease. *Eur. J. Biochem.* **237:** 6–15.

Hilbich, C., Kisters-Woike, B., Reed, J., Masters, C.L., and Beyreuther, K. 1991. Aggregation and secondary structure of synthetic amyloid βA4 peptides of Alzheimer's disease. *J. Mol. Biol.* **218:** 149–163.

Hou, L., Kang, I., Marchant, R.E., and Zagorski, M.G. 2002a. Methionine 35 oxidation reduces fibril assembly of the amyloid β-(1–42) peptide of Alzheimer's disease. *J. Biol. Chem.* **277:** 40173–40176.

Hou, L., Shao, H., and Zagorski, M.G. 2002b. Oxidation of Met35 exerts a profound effect on Aβ amyloidosis. *Neurobiol. Aging* **23:** S195.

Hou, L., Shao, H., Zhang, Y., Li, H., Menon, N.K., Neuhaus, E.B., Brewer, J.M., Byeon, I.-J.L., Ray, D.G., Vitek, M.P., et al. 2004. Solution NMR studies of the Aβ(1–40) and Aβ(1–42) peptides establish that the Met35 oxidation state affects the mechanism of amyloid formation. *J. Am. Chem. Soc.* **126:** 1992–2005.

Hubbard, S.J. 1998. The structural aspects of limited proteolysis of native proteins. *Biochim. Biophys. Acta* **1382:** 191–206.

Hutchinson, E.G. and Thornton, J.M. 1994. A revised set of potentials for β-turn formation in proteins. *Protein Sci.* **3:** 2207–2216.

Hwang, T.L. and Shaka, A.J. 1992. Cross relaxation without TOCSY—Transverse rotating-frame Overhauser effect spectroscopy. *J. Am. Chem. Soc.* **114:** 3157–3159.

Iwatsubo, T., Mann, D.M.A., Odaka, A., Suzuki, N., and Ihara, Y. 1995. Amyloid β Protein (Aβ) Deposition: Aβ42(43) precedes Aβ40 in Down syndrome. *Ann. Neurol.* **37:** 294–299.

Jarrett, J.T., Berger, E.P., and Lansbury Jr., P.T. 1993. The C terminus of the β protein is critical in amyloidogenesis. *Ann. N.Y. Acad. Sci.* **695:** 144–148.

Kamino, K., Orr, H.T., Payami, H., Wijsman, E.M., Alonso, E., Pulst, S.M., Anderson, L., O'dahl, S., Nemens, E., White, J.A., et al. 1992. Linkage and mutational analysis of familial Alzheimer disease kindreds for the APP gene region. *Am. J. Hum. Genet.* **51:** 998–1014.

Kheterpal, I., Williams, A., Murphy, C., Bledsoe, B., and Wetzel, R. 2001. Structural features of the Aβ amyloid fibril elucidated by limited proteolysis. *Biochemistry* **40:** 11757–11767.

Kheterpal, I., Lashuel, H.A., Hartley, D.M., Walz, T., Lansbury Jr., P.T. and Wetzel, R. 2003. Aβ protofibrils possess a stable core structure resistant to hydrogen exchange. *Biochemistry* **42:** 14092–14098.

Kirkitadze, M.D., Condron, M.M., and Teplow, D.B. 2001. Identification and characterization of key kinetic intermediates in amyloid β-protein fibrillogenesis. *J. Mol. Biol.* **312:** 1103–1119.

Kirkitadze, M.D., Bitan, G., and Teplow, D.B. 2002. Paradigm shifts in Alzheimer's disease and other neurodegenerative disorders: The emerging role of oligomeric assemblies. *J. Neurosci. Res.* **69:** 567–577.

Klein, W.L., Krafft, G.A., and Finch, C.E. 2001. Targeting small Aβ oligomers: The solution to an Alzheimer's disease conundrum? *Trends Neurosci.* **24:** 219–224.

Klein, W.L., Stine Jr., W.B., and Teplow, D.B. 2004. Small assemblies of unmodified amyloid β-protein are the proximate neurotoxin in Alzheimer's disease. *Neurobiol. Aging* **25:** 569–580.

Kusumoto, Y., Lomakin, A., Teplow, D.B., and Benedek, G.B. 1998. Temperature dependence of amyloid β-protein fibrillization. *Proc. Natl. Acad. Sci.* **95:** 12277–12282.

Laczko, I., Holly, S., Konya, Z., Soos, K., Varga, J.L., Hollosi, M., and Penke, B. 1994. Conformational mapping of amyloid peptides from the putative neurotoxic 25–35 region. *Biochem. Biophys. Res. Commun.* **205:** 120–126.

Lambert, M.P., Barlow, A.K., Chromy, B.A., Edwards, C., Freed, R., Liosatos, M., Morgan, T.E., Rozovsky, I., Trommer, B., Viola, K.L., et al. 1998. Diffusible, nonfibrillar ligands derived from $A\beta_{1-42}$ are potent central nervous system neurotoxins. *Proc. Natl. Acad. Sci.* **95:** 6448–6453.

Lazo, N.D. and Downing, D.T. 1998. Amyloid fibrils may be assembled from β-helical protofibrils. *Biochemistry* **37:** 1731–1735.

———. 1999. Fibril formation by amyloid-β proteins may involve β-helical protofibrils. *J. Pept. Res.* **53:** 633–640.

Le Châtelier, H. 1884. Sur un énoncé général des lois des équilibres chimiques. *Comptes Rendus* **99:** 786–789.

Lee, J.P., Stimson, E.R., Ghilardi, J.R., Mantyh, P.W., Lu, Y.A., Felix, A.M., Llanos, W., Behbin, A., Cummings, M., Vancriekinge, M., et al. 1995. ^{1}H NMR of Aβ amyloid peptide congeners in water solution. Conformational changes correlate with plaque competence. *Biochemistry* **34:** 5191–5200.

Levy, E., Carman, M.D., Fernandez-Madrid, I.J., Power, M.D., Lieberburg, I., van Duinen, S.G., Bots, G.T.A.M., Luyendijk, W., and Frangione, B. 1990. Mutation of the Alzheimer's disease amyloid gene in hereditary cerebral hemorrhage, Dutch-type. *Science* **248:** 1124–1126.

Lomakin, A., Chung, D.S., Benedek, G.B., Kirschner, D.A., and Teplow, D.B. 1996. On the nucleation and growth of amyloid β-protein fibrils: Detection of nuclei and quantitation of rate constants. *Proc. Natl. Acad. Sci.* **93:** 1125–1129.

Ma, B. and Nussinov, R. 2002. Stabilities and conformations of Alzheimer's β-amyloid peptide oligomers ($A\beta_{16-22}$, $A\beta_{16-35}$, and $A\beta_{10-35}$): Sequence effects. *Proc. Natl. Acad. Sci.* **99:** 14126–14131.

Marqusee, S. and Baldwin, R.L. 1987. Helix stabilization by Glu-...Lys+ salt bridges in short peptides of de novo design. *Proc. Natl. Acad. Sci.* **84:** 8898–8902.

Massi, F. and Straub, J.E. 2001. Energy landscape theory for Alzheimer's amyloid β-peptide fibril elongation. *Proteins* **42:** 217–229.

Maynard, A.J., Sharman, G.J., and Searle, M.S. 1998. Origin of β-hairpin stability in solution: Structural and thermodynamic analysis of the folding of model peptide supports hydrophobic stabilization in water. *J. Am. Chem. Soc.* **120:** 1996–2007.

Melchor, J.P., McVoy, L., and Van Nostrand, W.E. 2000. Charge alterations of E22 enhance the pathogenic properties of the amyloid β-protein. *J. Neurochem.* **74:** 2209–2212.

Monti, M., Garolla di Bard, B.L., Calloni, G., Chiti, F., Amoresano, A., Ramponi, G., and Pucci, P. 2004. The regions of the sequence most exposed to the solvent within the amyloidogenic state of a protein initiate the aggregation process. *J. Mol. Biol.* **336:** 253–262.

Neira, J.L. and Fersht, A.R. 1996. An NMR study on the β-hairpin region of barnase. *Fold. Des.* **1:** 231–241.

Nilsberth, C., Westlind-Danielsson, A., Eckman, C.B., Condron, M.M., Axelman, K., Forsell, C., Stenh, C., Luthman, J., Teplow, D.B., Younkin, S.G., et al. 2001. The "Arctic" APP mutation (E693G) causes Alzheimer's disease by enhanced Aβ protofibril formation. *Nat. Neurosci.* **4:** 887–893.

Oda, T., Wals, P., Osterburg, H.H., Johnson, S.A., Pasinetti, G.M., Morgan, T.E., Rozovsky, I., Stine, W.B., Snyder, S.W., Holzman, T.F., et al. 1995. Clusterin (ApoJ) alters the aggregation of amyloid β-peptide ($A\beta_{1-42}$) and forms slowly sedimenting Aβ complexes that cause oxidative stress. *Exp. Neurol.* **136:** 22–31.

Päiviö, A., Jarvet, J., Graslund, A., Lannfelt, L., and Westlind-Danielsson, A. 2004. Unique physicochemical profile of β-amyloid peptide variant Aβ1–40E22G protofibrils: Conceivable neuropathogen in Arctic mutant carriers. *J. Mol. Biol.* **339:** 145–159.

Palmblad, M., Westlind-Danielsson, A., and Bergquist, J. 2002. Oxidation of methionine 35 attenuates formation of amyloid β-peptide 1–40 oligomers. *J. Biol. Chem.* **277:** 19506–19510.

Petkova, A.T., Ishii, Y., Balbach, J.J., Antzutkin, O.N., Leapman, R.D., Delaglio, F., and Tycko, R. 2002. A structural model for Alzheimer's β-amyloid fibrils based on experimental constraints from solid state NMR. *Proc. Natl. Acad. Sci.* **99:** 16742–16747.

Polverino de Laureto, P., Taddei, N., Frare, E., Capanni, C., Costantini, S., Zurdo, J., Chiti, F., Dobson, C.M., and Fontana, A. 2003. Protein aggregation and amyloid fibril formation by an SH3 domain probed by limited proteolysis. *J. Mol. Biol.* **334:** 129–141.

Roberts, G.C.K. 1993. *NMR of macromolecules: a practical approach*. IRL Press/Oxford University Press, Oxford.

Schechter, I. and Berger, A. 1967. On the size of the active site in proteases. I. Papain. *Biochem. Biophys. Res. Commun.* **27:** 157–162.

Sciarretta, K.L., Gordon, D.J., Petkova, A.T., Tycko, R., and Meredith, S.C. 2005. Aβ40-lactam(D23/K28) models a conformation highly favorable for nucleation of amyloid. *Biochemistry*. (in press).

Seilheimer, B., Bohrmann, B., Bondolfi, L., Muller, F., Stuber, D., and Döbeli, H. 1997. The toxicity of the Alzheimer's β-amyloid peptide correlates with a distinct fiber morphology. *J. Struct. Biol.* **119:** 59–71.

Seubert, P., Vigo-Pelfrey, C., Esch, F., Lee, M., Dovey, H., Davis, D., Sinha, S., Schlossmacher, M.G., Whaley, J., Swindlehurst, C., et al. 1992. Isolation and quantitation of soluble Alzheimer's β-peptide from biological fluids. *Nature* **359:** 325–327.

Shao, H.Y., Jao, S.C., Ma, K., and Zagorski, M.G. 1999. Solution structures of micelle-bound amyloid β-(1–40) and β-(1–42) peptides of Alzheimer's disease. *J. Mol. Biol.* **285:** 755–773.

Shoji, M., Golde, T.E., Ghiso, J., Cheung, T.T., Estus, S., Shaffer, L.M., Cai, X., McKay, D.M., Tintner, R., Frangione, B., et al. 1992. Production of the Alzheimer amyloid β protein by normal proteolytic processing. *Science* **258:** 126–129.

Snyder, S.W., Ladror, U.S., Wade, W.S., Wang, G.T., Barrett, L.W., Matayoshi, E.D., Huffaker, H.J., Krafft, G.A., and Holzman, T.F.

1994. Amyloid-β aggregation: Selective inhibition of aggregation in mixtures of amyloid with different chain lengths. *Biophys. J.* **67:** 1216–1228.

Sorimachi, K., Craik, D.J., Lloyd, E.J., Beyreuther, K., and Masters, C.L. 1990. Identification of a β-turn in the tertiary structure of a peptide fragment of the Alzheimer amyloid protein. *Biochem. Int.* **22:** 447–454.

Soto, C., Castaño, E.M., Frangione, B., and Inestrosa, N.C. 1995. The α-helical to β-strand transition in the amino-terminal fragment of the amyloid β-peptide modulates amyloid formation. *J. Biol. Chem.* **270:** 3063–3067.

Sreerama, N. and Woody, R.W. 2000. Estimation of protein secondary structure from circular dichroism spectra: Comparison of CONTIN, SELCON, and CDSSTR methods with an expanded reference set. *Anal. Biochem.* **287:** 252–260.

Sticht, H., Bayer, P., Willbold, D., Dames, S., Hilbich, C., Beyreuther, K., Frank, R.W., and Rosch, P. 1995. Structure of amyloid A4-(1–40)-peptide of Alzheimer's disease. *Eur. J. Biochem.* **233:** 293–298.

Sun, X.D., Mo, Z.L., Taylor, B.M., and Epps, D.E. 2003. A slowly formed transient conformer of Aβ(1–40) is toxic to inward channels of dissociated hippocampal and cortical neurons of rats. *Neurobiol. Dis.* **14:** 567–578.

Tagliavini, F., Rossi, G., Padovani, A., Magoni, M., Andora, G., Sgarzi, M., Bizzi, A., Savioardo, M., Carella, F., Morbin, M., et al. 1999. A new βPP mutation related to hereditary cerebral hemorrhage. *Alzheimer's Rep. (Suppl.)* **2:** S28.

Taylor, B.M., Sarver, R.W., Fici, G., Poorman, R.A., Lutzke, B.S., Molinari, A., Kawabe, T., Kappenman, K., Buhl, A.E., and Epps, D.E. 2003. Spontaneous aggregation and cytotoxicity of the β-amyloid $A\beta^{1-40}$: A kinetic model. *J. Protein Chem.* **22:** 31–40.

Teplow, D.B. 1998. Structural and kinetic features of amyloid β-protein fibrillogenesis. *Amyloid* **5:** 121–142.

Teplow, D.B., Lomakin, A., Benedek, G.B., Kirschner, D.A., and Walsh, D.M. 1997. Effects of β-protein mutations on amyloid fibril nucleation and elongation. In *Alzheimer's disease: Biology, diagnosis and therapeutics* (eds. K. Iqbal et al.), pp. 311–319. John Wiley & Sons Ltd., Chichester, England.

Tsubuki, S., Takaki, Y., and Saido, T.C. 2003. Dutch, Flemish, Italian, and Arctic mutations of APP and resistance of Aβ to physiologically relevant proteolytic degradation. *Lancet* **361:** 1957–1958.

Tycko, R. 2004. Progress towards a molecular-level structural understanding of amyloid fibrils. *Curr. Opin. Struct. Biol.* **14:** 1–8.

Urbanc, B., Cruz, L., Yun, S., Buldyrev, S.V., Bitan, G., Teplow, D.B., and Stanley, H.E. 2004. In silico study of amyloid β-protein folding and oligomerization. *Proc. Natl. Acad. Sci.* **101:** 17345–17350.

Walsh, D.M., Lomakin, A., Benedek, G.B., Condron, M.M., and Teplow, D.B. 1997. Amyloid β-protein fibrillogenesis—Detection of a protofibrillar intermediate. *J. Biol. Chem.* **272:** 22364–22372.

Walsh, D.M., Hartley, D.M., Kusumoto, Y., Fezoui, Y., Condron, M.M., Lomakin, A., Benedek, G.B., Selkoe, D.J., and Teplow, D.B. 1999. Amyloid β-protein fibrillogenesis—Structure and biological activity of protofibrillar intermediates. *J. Biol. Chem.* **274:** 25945–25952.

Walsh, D.M., Klyubin, I., Fadeeva, J.V., Cullen, W.K., Anwyl, R., Wolfe, M.S., Rowan, M.J., and Selkoe, D.J. 2002. Naturally secreted oligomers of amyloid β protein potently inhibit hippocampal long-term potentiation *in vivo*. *Nature* **416:** 535–539.

Watson, A.A., Fairlie, D.P., and Craik, D.J. 1998. Solution structure of methionine-oxidized amyloid β-peptide (1–40)—Does oxidation affect conformational switching? *Biochemistry* **37:** 12700–12706.

Williams, A.D., Portelius, E., Kheterpal, I., Guo, J.-T., Cook, K.D., Xu, Y., and Wetzel, R. 2004. Mapping Aβ amyloid fibril secondary structure using scanning proline mutagenesis. *J. Mol. Biol.* **335:** 833–842.

Wisniewski, T., Ghiso, J., and Frangione, B. 1991. Peptides homologous to the amyloid protein of Alzheimer's disease containing a glutamine for glutamic acid substitution have accelerated amyloid fibril formation. *Biochem. Biophys. Res. Commun.* **179:** 1247–1254.

Wurth, C., Guimard, N.K., and Hecht, M.H. 2002. Mutations that reduce aggregation of the Alzheimer's Aβ42 peptide: An unbiased search for the sequence determinants of Aβ amyloidogenesis. *J. Mol. Biol.* **319:** 1279–1290.

Wüthrich, K. 1986. *NMR of proteins and nucleic acids*. John Wiley & Sons, New York.

Younkin, S.G. 1995. Evidence that Aβ42 is the real culprit in Alzheimer's disease. *Ann. Neurol.* **37:** 287–288.

Zagorski, M.G., Shao, H., Ma, K., Yang, J., Li, H., Zeng, H., Zhang, Y., and Papolla, M. 2000. Aβ(1–40) and Aβ(1–42) adopt remarkably stable monomeric and extended structures in water solution at neutral pH. *Neurobiol. Aging* **21:** S10–S11 (Abstract 48).

Zhang, S., Iwata, K., Lachenmann, M.J., Peng, J.W., Li, S., Stimson, E.R., Lu, Y., Felix, A.M., Maggio, J.E., and Lee, J.P. 2000. The Alzheimer's peptide Aβ adopts a collapsed coil structure in water. *J. Struct. Biol.* **130:** 130–141.